aerospace

MDPI

Article

Modeling the Transient Dynamics of Arresting Hooks and Cables through the Parameter Inversion Method

Long Li [1,2], Yiming Peng [1,2,*], Yifeng Wang [1,2], Xiaohui Wei [1,2] and Hong Nie [1,2]

[1] State Key Laboratory of Mechanics and Control of for Aerospace Structures, Nanjing University of Aeronautics and Astronautics, No. 29 Yudao Street, Nanjing 210016, China; lilong2@nuaa.edu.cn (L.L.)
[2] Key Laboratory of Fundamental Science for National Defense-Advanced Design Technology of Flight Vehicle, Nanjing University of Aeronautics and Astronautics, Nanjing 210016, China
* Correspondence: yimingpeng@nuaa.edu.cn

Abstract: Arresting gear systems play a vital role in carrier-based aircraft landing. In order to accurately understand the process of arresting hook and cable, this study introduces a parameter inversion method to model the arresting cable and applies it to the transient dynamics model of the arresting hook and cable. The feasibility of the arresting cable model and its application to the transient dynamics model of the arresting hook and cable are validated through arresting hook and cable impact tests. The study compares three different models of arresting cables for simulation results and concludes that assuming the arresting cable to be a beam with metal elastic parameters during the modeling process cannot ignore the influence of the cable's torsional and bending stiffness on the modeling. The study also investigates the dynamic response of the arresting hook during the aircraft arrestment and hooking process and concludes that the stress peak of the hook arm is much lower throughout the entire arrestment process than at the moment of hooking the cable. The study further identifies factors that affect the stress on the arresting hook arm, such as the aircraft's yaw angle, deck angle, cruising speed, and the initial position of the arresting hook and cable before engagement. The research results have significant implications for improving the design optimization of the structural strength of the functional components of the naval aircraft arresting system and provide theoretical guidance and technical reserves for subsequent related studies.

Keywords: arresting hook; arresting cable; parameter inversion; finite element analysis; dynamic response

Citation: Li, L.; Peng, Y.; Wang, Y.; Wei, X.; Nie, H. Modeling the Transient Dynamics of Arresting Hooks and Cables through the Parameter Inversion Method. *Aerospace* **2024**, *11*, 20. https://doi.org/10.3390/aerospace11010020

Academic Editor: Nguyen Dinh Duc

Received: 6 November 2023
Revised: 18 December 2023
Accepted: 21 December 2023
Published: 25 December 2023

1. Introduction

The arresting hook is one of the most important characteristic components of carrier-based aircraft. Together with the arresting cable, they are critical connecting components between the aircraft and the aircraft carrier. The role of the arresting hook and arresting cable in carrier-based aircraft landing is extremely important. According to the distribution data of aircraft accidents on U.S. carriers, although the landing phase of carrier-based aircraft only accounts for 4% of its mission cycle time, the number of accidents accounts for 44.4% of all accidents [1]. The structural strength of the arresting hook and arresting cable directly affects the maximum takeoff and landing weight and service life of carrier-based aircraft. Therefore, studying their dynamic response issues is of great guiding significance for the development and application of carrier-based aircraft.

Research on the dynamic response of aircraft arresting hooks and arresting cables has a history of several decades, and related studies have become quite mature. The US military has established a series of military specifications, among which MIL-STD-2066 [2] provides load variation rules for aircraft arresting hooks under different arresting systems based on a large amount of test data. Yang et al. [3] measured the load of an aircraft arresting hook using strain gauges during flight tests and established a three-directional load measurement model for aircraft arresting hooks. Zhang et al. [4] proposed a static

strength test design method for arresting hooks applicable to engineering tests and verified the effectiveness of the method through static strength tests of a certain type of aircraft arresting hook. Research on arresting cables has also been carried out for several decades, focusing mainly on theoretical models such as stress wave propagation and bending wave. Ringleb FO et al. [5] were the first to systematically study the dynamic problems of cables, established the wave equation of stress propagation, and explained the reflection of transverse waves and stress waves in arresting cables. Gibson et al. [6–8] considered more influencing factors on this basis and established a more comprehensive design theory for arresting cables. ADEC Corporation [9] proposed the wave propagation load theory for calculating the strain dynamic load of arresting cables, which has been applied in engineering. Gao et al. [9] used the wave propagation load theory to analyze the influence of different cable materials on the strain dynamic load of arresting cables and verified through examples that the size of aircraft arresting cable strain dynamic load is closely related to the configuration of ground arresting devices, cable materials, and the eccentricity of aircraft landing.

There is currently limited research on the transient dynamic response of arresting hook and pendant impact due to the difficulty in accurately modeling the special construction and large bending deformation effects of the arresting cable. In recent years, the development of computer-aided tools has provided new avenues for simulating and studying ropes. Liang et al. [10,11] used the finite element method to establish a collision dynamics model for the arrestment system and found that there were continuous attenuating stress waves between the arresting cable and deck pulley. When the first reflected wave from the deck pulley reached the hook engagement point, the arresting force reached its maximum value. Shen et al. [12,13] developed large displacement single elements with contact and collision capabilities based on the absolute nodal coordinate formulation, providing a computational means for the design and optimization of full-size carrier-based aircraft arrestment systems. Zhang Q [14] proposed a new method for the impact test of arresting hook and pendant and designed a corresponding experimental platform. He also conducted experiments on the collision of a certain type of carrier-based aircraft arresting hook and pendant using the platform, providing an important experimental method for the design of carrier-based aircraft arresting systems. Dang et al. [15] used the finite element method to study the dynamic response of carrier-based aircraft arresting hooks during the arrestment and landing process. This study provides an important basis for multi-impulse dynamic analysis of the arresting hook. It is worth noting that previous theoretical and simulation studies of the arresting cable ignored the large bending deformation that occurs during the hanging process of the cable and the special construction of the steel wire, which resulted in low accuracy of the arresting cable model and inability to obtain accurate simulation models of hook and pendant impact.

This paper proposes a precise modeling method for the arresting cable based on the parameter inversion method [16]. The lack of accurate modeling of the special structure and large bending deformation of the arresting cable is the main reason for the limited research on the transient dynamic response of the arresting hook on the cable. In recent years, the development of computer-aided tools has provided new avenues for simulating and studying ropes. The authors first establish a simplified finite element model of the arresting cable considering the cable construction, and then use the key parameters of steel cable bending obtained from a three-point bending test to improve the arresting cable model using the parameter inversion method. They then establish a finite element model of the arresting hook and verify the accuracy of the simulation model using static loading tests. Finally, they establish a dynamic analysis model for the impact of the arresting hook on the cable and use corresponding experiments to validate the model's effectiveness. The study also investigates the impact of different arresting cable parameters and modeling methods on the transient dynamic behavior during the arresting process and the necessity of considering the cable bending. The results provide a more reasonable theoretical basis

for the structural strength design of the arresting hook and the precise modeling method of the arresting cable and have important engineering value.

2. Research on Modeling Method of Arresting Cable

2.1. Basic Assumption

The arresting cable has a complex structure and is usually formed by twisting many steel and fiber wires together. Creating a micro-scale model of the arresting cable in finite element software requires a lot of computational resources, which leads many researchers to simplify the arresting cable when studying the mechanical properties of the arresting hook and cable.

Due to the longitudinal length of the arresting cable being much larger than its transverse diameter, the bending stiffness or shear stiffness of the cable is usually ignored in structural design, and only the axial tensile bearing capacity of the cable is considered. In current research on arresting systems, the complex cable structure is often simplified as a metal elastic beam or rod for analysis. This modeling method neglects the structural characteristics of the real arresting cable, leading to significant mechanical performance deviations in simulation results.

To address this issue, this paper proposes a reasonable simplification of the arresting cable, by introducing a model that considers its bending stiffness. Based on the physical arresting cable studied, bending stiffness tests were conducted and the obtained data were used to perform parameter inversion on the cable model, ultimately resulting in a simplified arresting cable model that considers bending stiffness. The specifications of the arresting cable studied in this paper are shown in Table 1.

1. To reduce the difficulty of modeling the cable, while ensuring the accuracy of the model, the following assumptions are made in this paper;
2. The twist rate of the mooring cable is zero during manufacturing and use;
3. The frictional force between the steel wires in the cable is large enough that wire slippage can be ignored;
4. The torsional characteristics of the cable are ignored during use;
5. The cable is divided into material zones, and the core and outer strands of the cable are treated as a whole, ignoring the gaps between the metal wires.

Table 1. Arresting cable specifications.

Arresting Cable Diameter	Cable Core Diameter	Cable Core Material	Side Strand Diameter	Number of Side Strand	Side Wire Diameter	Side Wire Material	Manufacture Method
39 mm	13.8 mm	nylon	12.6 mm	37	1.8 mm	1065 (ASTM)	right lang lay

Based on these assumptions, the arresting cable model established in this paper is shown in Figure 1. The model is divided into layers based on the material, with the inner layer being the material properties of the nylon core with an elastic modulus E_{nylon}, and the outer layer being the equivalent material properties of the metal with an equivalent elastic modulus E^* and a line density of ρ^*.

2.2. Experimental Study on the Bending Stiffness of Arresting Cables

The experimental principle of steel cable bending stiffness is shown in Figure 2, based on the three-point bending method [17]. There are three points (rollers) in contact with the steel cable on the test bench, where rollers A and B are fixed, and roller C can move up and down. Under the action of the tangential load applied by roller C, the tested steel cable will undergo bending deformation on the bending stiffness test bench, and the bending stiffness of the cable can be measured accordingly.

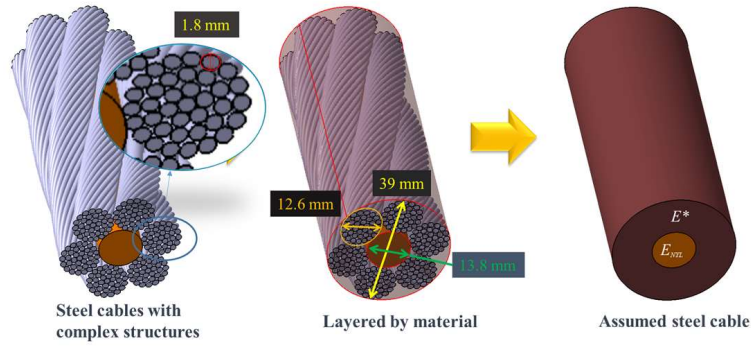

Figure 1. The process of building the equivalent wire cable model.

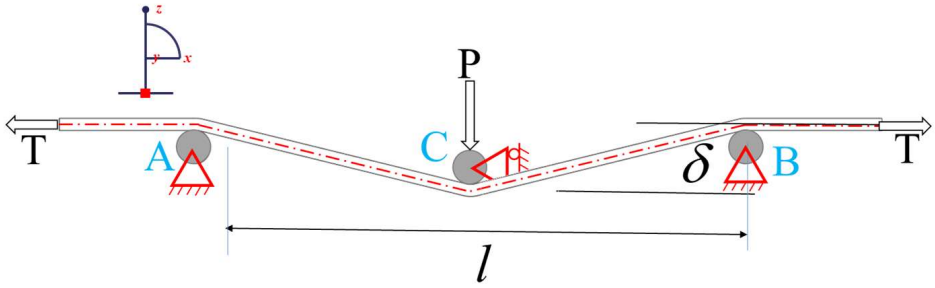

Figure 2. Principle of steel cable bending stiffness determination.

As shown in Figure 2, when the steel cable is subjected to tensile force $\boldsymbol{T}$ at both ends, under the action of the tangential load applied by the roller $\boldsymbol{C}$ in the downward direction relative to A and B, bending deformation and displacement δ and pressure $\boldsymbol{P}$ will occur. When the weight of the roller is much smaller than the tangential load, the theoretical model for the bending stiffness of the obstruction cable can be obtained according to the literature [17].

$$\sqrt{E_s I_s} = \frac{Pl - 4T\delta}{3P}\sqrt{T}, \tag{1}$$

Equation (1) shows that the bending stiffness of the cable barrier can be determined by using the displacement, pressure, and tensile force data obtained from the experiment. Here, $E_s I_s$ is the bending stiffness of the steel cable, P is the pressure applied by the roller $\boldsymbol{C}$, T is the tensile force at both ends of the steel cable, and δ is the tangential displacement of the roller C.

If T and $\boldsymbol{l}$ are constant, the displacement and pressure signals are measured twice assuming that $E_s I_s$ is constant.

If T and $\boldsymbol{l}$ are constant, and assuming $E_s I_s$ remains constant, with displacement and pressure measured twice as δ_1,δ_2 and P_1,P_2, respectively, then:

$$\sqrt{E_s I_s} = \frac{P_1 l - 4T\delta_1}{3P_1}\sqrt{T} = \frac{P_2 l - 4T\delta_2}{3P_2}\sqrt{T}, \tag{2}$$

Simplified

$$\frac{\delta_1}{P_1} = \frac{\delta_2}{P_2} = k^* = \frac{l - 3\sqrt{\frac{E_S I_S}{T}}}{4T}, \tag{3}$$

Based on the above analysis, it can be concluded that under the condition of constant tensile force and bending stiffness of the rope, the tangential load and tangential displacement are proportional, and the proportion is related to the tensile force and bending stiffness of the rope.

According to this principle, a bending stiffness test rig for the restraining rope was built in this study, as shown in Figure 3. The distance between roller A, B, and C, the tensile force T at both ends of the cable, and the mass of the rollers W can be adjusted. The

displacement signal δ and pressure signal P can be measured by sensors. By adjusting the axial tension at both ends of the rope and applying a pressure load P in the middle of the cable, the tangential displacement and pressure data of the steel cable can be obtained under different axial tension.

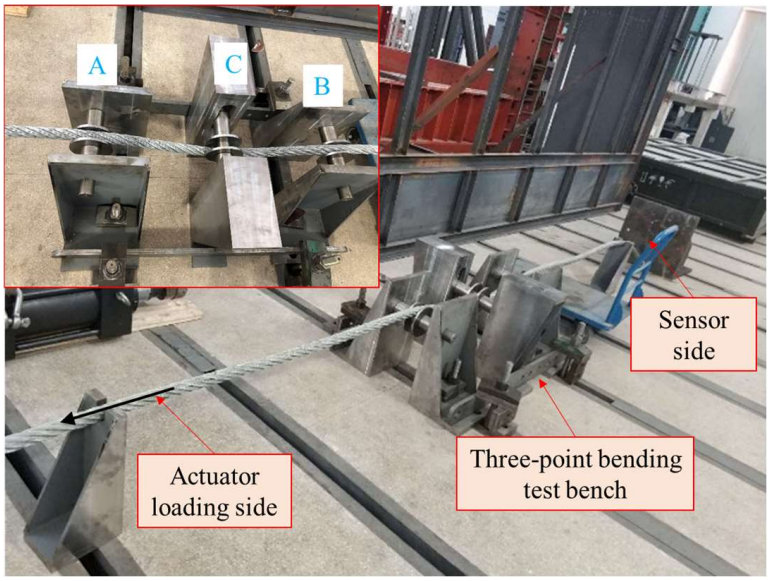

Figure 3. Steel cable bending stiffness test bench.

2.3. Inversion of Bending Stiffness Parameter of Arresting Cable

In this study, a simulation model of the arresting cable was established using the finite element software ABAQUS [18]. The cable has a length of 10,000 mm and is modeled using C3D8R elements with a size of 9 mm, resulting in a total of 31,575 elements and 37,980 nodes. The variable parameters, including the wheel distance l, roller weight W, and tension T, are consistent with those used in the previous experiments. The cable core is made of nylon with an elastic modulus E_{nylon}, and the outer layer of the cable is assumed to be an isotropic material with an elastic modulus of E^* and a density of ρ^*, as shown in Figure 4. The cable core is made of nylon, and the outer layer of the cable is assumed to be an isotropic material with an elastic modulus of E^* and a density of ρ^*, as shown in Figure 4. The simulation model neglects the effects of rope lay length and gaps (i.e., the variation of the overall I_s of the arresting rope) and only considers the influence of the elastic parameter E^* on the bending effect.

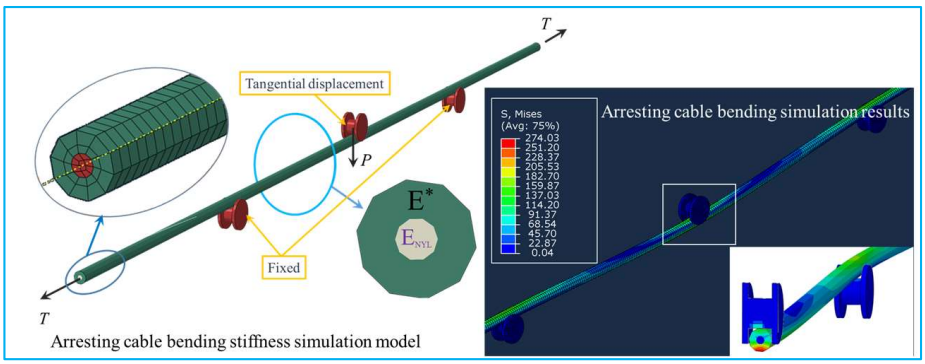

Figure 4. Arresting cable bending stiffness simulation model and results.

The parameters in the finite element model of the arresting cable are inverted by utilizing the bending test data of the cable, as shown in Figure 5. The computation process is conducted with the Isight 2017, as demonstrated in Figure 6.

(1) The change curves of tangential displacement and pressure under different tensions are obtained through three-point bending tests of the arresting cable;
(2) A finite element model of the arresting cable is established;
(3) By conducting multiple simulations, an approximate model of the simplified arresting cable is obtained;
(4) The displacement and load data collected from experiments are used as calibration curves. The elastic parameter E^* of the outer material in the simulation model is defined as the optimization parameter. The Sum of Squared Differences (SSD) algorithm, which is a common algorithm used in image matching, is used for optimization inversion. The approximate model calculates the simulation result curve that approaches the calibration curve, and a model with mechanical properties similar to the actual object is obtained.

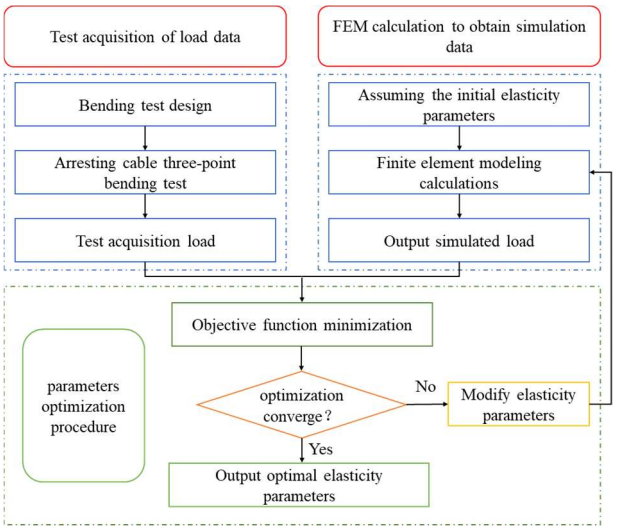

Figure 5. The inversion process of elastic parameters of arresting cable.

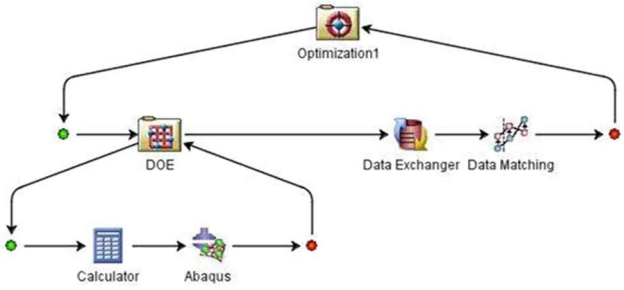

Figure 6. Parameter inversion process simulation platform.

The SSD algorithm, which is a common algorithm used in image matching, is often used for block matching of images, calculating the sum of squared differences of the absolute value of the difference between corresponding pixel values to evaluate the similarity of two image blocks. The optimization mathematical equation is as follows:

$$D(i,j) = \sum_{s=1}^{M}\sum_{t=1}^{N}\left[A(i+s-1, j+t-1) - B(s,t)\right]^2, \quad (4)$$

$D(i,j)$ is the sum of squared differences between two images or regions; $A(i+s-1, j+t-1)$ denotes the pixel intensity at coordinates (x, y) in image A; $B(s, t)$ signifies the pixel intensity at location (x, y) in the template or comparison region. The summation encompasses all pixel coordinates (x, y) shared between A and B.

Essentially, SSD computes the total of squared intensity differences between pixels of two images or areas. This metric gauges similarity: a lower SSD indicates greater resemblance between the images or areas. SSD proves invaluable in contexts requiring exact pixel-level alignment, like depth calculation in stereo vision, motion tracking, and identifying objects.

In this study, a simulation model of the arresting cable was established using the finite element software ABAQUS [18]. The cable has a length of 10,000 mm and is modeled using C3D8R elements with a size of 9 mm, resulting in a total of 31,575 elements and 37,980 nodes. The variable parameters, including the wheel distance l, roller weight W, and tension T, are consistent with those used in the previous experiments. The cable core is made of nylon, and the outer layer of the cable is assumed to be an isotropic material with an elastic modulus of E^* and a density of ρ^*, as shown in Figure 4. The simulation model neglects the effects of rope lay length and gaps (i.e., the variation of the overall I_s of the arresting rope) and only considers the influence of the elastic parameter E^* on the bending effect.

Finally, the external elastic parameter E^* of the outer layer corresponding to the interception cable under different tensions was obtained through parameter inversion [19], and the results are shown in Table 2. The optimal parameter E^* was then substituted back into the finite element model, and the results of the experimental and simulated loads and displacements were compared, as shown in Figure 7.

Table 2. Parameter inversion fitting results.

Case Number	Tensile Force at Both Ends/N	Elastic Parameter E^*/MPa
1	10,000	12,850
2	20,000	22,160
3	30,000	30,172
4	40,000	38,892
5	50,000	43,128
6	60,000	45,049

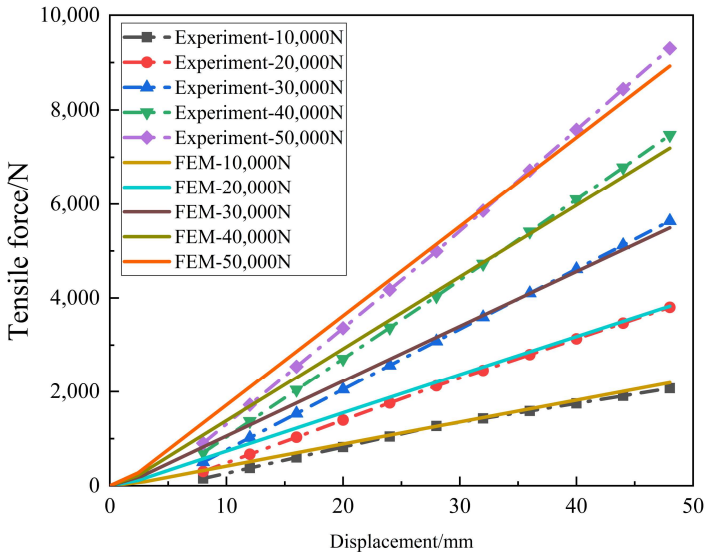

Figure 7. The optimal solution diagram of the test and simulation load-displacement curve.

The experiments in reference [19] and the research in reference [20] both indicate that the friction between steel cables limits the relative slip between them. When subjected to transverse loads that cause bending, shear forces occur along the axial direction inside the cable bundle. When the bending is small, the axial shear force is smaller than the friction between the steel cables, and there is a tendency for relative slip between the cables.

When the bending is large, the shear force exceeds the accumulated friction along the axial direction, causing a large segment of cables to enter a parallel sliding state, exhibiting a bending stiffness that is almost a constant value. Therefore, in this paper, it is assumed that the bending stiffness of the arresting cable is E = 43,000 MPa when subjected to impact and remains unchanged during the impact process.

3. Analysis of Mechanical Performance Parameters of Arresting Hook and Cable

3.1. Arresting Hook Mechanical Performance Parameters

This study focuses on the Y-shaped tube structure of the hook arm of the arresting hook. Due to the harsh working environment of the arresting hook, it is inconvenient to place strain gauges at the hook head to monitor its strain state during the arresting hook test. Therefore, in this study, strain gauges were arranged on one side of the symmetrical hook arm of the Y-shaped structure to monitor the strain at this point, as shown in Figure 8, which can detect the influence of stress waves generated by the hanging cable impact on the hook arm.

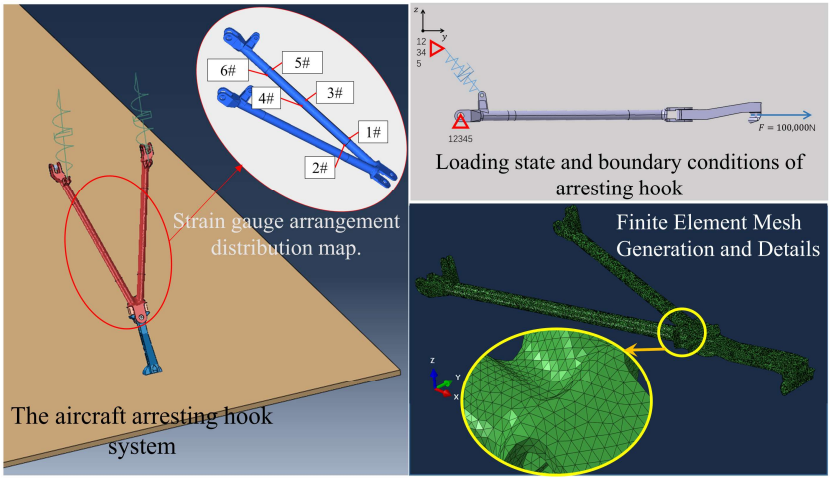

Figure 8. Arresting hook model building.

To verify the effectiveness of the steel cable in the transient dynamic simulation model of the arresting hook, the arresting hook finite element model was verified separately. The outer structure of the arresting hook is shown in Figure 8. The hook arm material of the arresting hook is AerMet 100 steel, and its related parameters [21] are shown in Table 3.

Table 3. Mechanical property of A100 steel.

E (MPa)	$\sigma_{0.2}$ (MPa)	σ_b (MPa)	δ_5 (%)	Ψ (%)	Rupt.ε_p
1925.60	1776.38	2102.93	12.46	62.0	0.1108

The arresting hook possesses intricate structural characteristics, with element types including C3D8R and C3D4, whereas the element at the hook arm is a C3D8R. The simulation model's boundary conditions encompass the intersection point of the two fuselages of the articulated arresting hook. The hook can rotate around this intersection point within the O-xy plane. Additionally, an axial force of 100,000 N is applied along the hook at the hook head position, as illustrated in Figure 8.

The simulation results for strain at the hook arm monitoring point were obtained through finite element analysis, and corresponding strain test results were acquired through static load tests on the arresting hook, as depicted in Figure 9. A comparison of the two sets of results is presented in Table 4, revealing that the maximum strain error value is less than 6%. This confirms the validity of the established finite element model for the arresting hook.

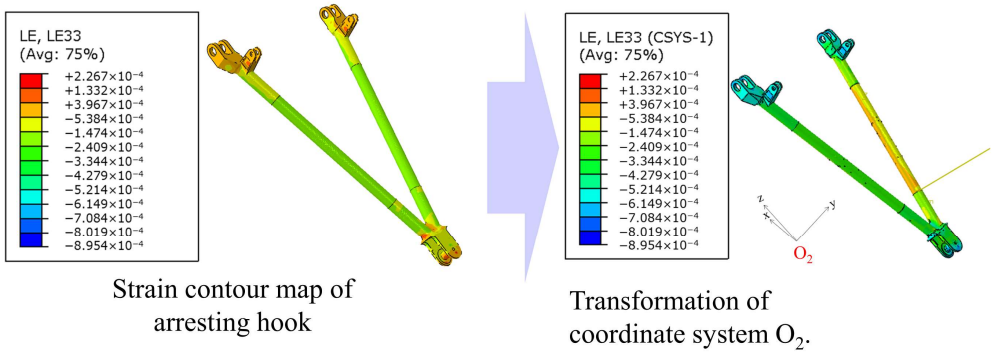

Figure 9. Strain results of the arresting hook.

Table 4. Verification of mechanical property of arresting hook.

Strain Gauge Location	Simulation (με)	Experiment (με)	Error Value
1#	234.25	228.25	2.63%
2#	375.48	394.62	4.85%
3#	200.18	210.03	4.69%
4#	423.71	422.13	0.37%
5#	144.16	152.45	5.43%
6#	480.24	508.04	5.47%

3.2. Arresting Cable Mechanical Performance Parameters

In this paper, the elastic modulus of the arresting cable is assumed to be E^* = 45,049 MPa. Based on the linear density and cross-sectional area of the arresting cable, the equivalent density $\rho^* = 5450\ \mathrm{kg/m^3}$ is obtained. The material properties of the cable model established in the end are shown in Table 5.

Table 5. Material parameters of steel cables obtained by parametric inversion.

Arresting Cable Parts	Density ρ kg/m^3	Elastic Modulus E/MPa	Poisson's Ratio ν
Arresting cable core	1000	1400	0.4
Arresting cable outer layer	5450	45,049	0.31

3.3. Arresting Cable Mechanical Performance Parameters

A transient dynamic model of the process of the arresting hook and arresting cable impact was established using the explicit dynamics function of the finite element software ABAQUS 6.14-3, as shown in Figure 10. The validity and mechanical performance of the mesh of the arresting hook have been verified in Section 3.1, and the model and parameters of the arresting cable were confirmed by parameter inversion in the previous section. The weight of the carrier-based aircraft was approximately 22 tons, and the aircraft had an angle of attack of 6° before engaging the arresting cable, with an angle of 62° between the arresting hook and the carrier deck. The buffers of the arresting hook and landing gear of the aircraft were replaced by non-linear elastic damping springs. The model ignored the effects of preconditions such as the pressure cable of the landing gear and the collision between the arresting hook and the deck, and the arresting was completed symmetrically. By assigning velocities to the center of gravity of the aircraft and the arresting hook, the transient dynamic performance of the arresting hook and arresting cable impact was obtained. The speed parameters of the carrier-based aircraft are shown in Table 6.

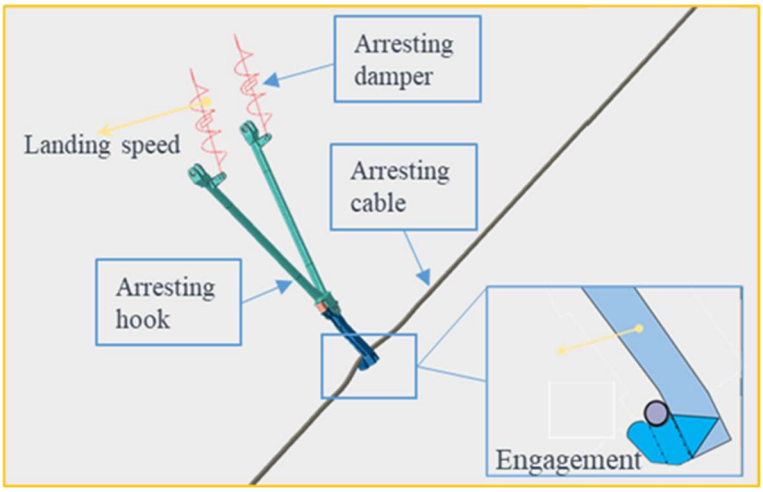

Figure 10. A transient dynamic finite element model of the arresting hook and arresting cable impact process.

Table 6. Landing parameters of carrier-based aircraft.

Case Number	Sinking Velocity (m/s)	Horizontal Velocity (m/s)	YawAngle (°)
1	3.5	41.15	6
2	3.5	51.44	6
3	3.5	61.73	6

To validate the feasibility of using parameter inversion to establish the interception cable model and applying it to the transient dynamic model of the interception hook and cable, this paper introduced an interception hook and cable impact test to verify the accuracy of the simulation model. The interception hook and cable impact test rig was the same as that in reference [14]. Since the load was not transmitted to the aircraft body at the moment when the interception hook and cable engaged, only the interception hook was given the landing speed and simulated with two speed components, i.e., the horizontal velocity and the descent velocity. The test scheme is shown in Figure 11. The simulation of the aircraft's descent speed was achieved by suspending the interception hook on a crane and allowing it to fall vertically from a certain height, while the simulation of the aircraft's horizontal speed was achieved by high-speed rotation of the cable system. The interception cable's tangential speed was used at the moment of impact between the hook and cable. The landing parameters of the aircraft were consistent with those in Table 6.

The previous section introduced the simulation and experimental testing of the strain monitoring for the intercept hook and hanging cable. In this section, we will compare the strain monitoring results under the same working conditions. All strain results are the axial strains in the local coordinate system O_2-xyz along the Z-axis, where the Z-axis of the local coordinate system is coaxial with the axis of the hook arm, and the XY plane is perpendicular to the hook arm, as shown in Figure 9. By comparing the time-varying strain curves of the six positions, it is found that the simulation results and experimental results have similar trends, especially the curve at the lower end of the hook arm is almost identical, as shown in Figure 12. Positions 1#, 3#, and 5# are the locations of the strain on the upper surface of the hook arm, and positions 2#, 4#, and 6# are the locations of the strain on the lower surface of the hook arm. The strains on the upper surface are all negative, while the strains on the lower surface are all positive, indicating that the hook arm underwent upward bending deformation during the impact period. Comparing the peak strain values of the intercept hook and hanging cable, the maximum error is no more than 10%, as shown in Table 7, which indicates that the modeling method of inverse analysis

of the intercept cable parameters is effective and can be applied to the transient dynamic model of the intercept hook and hanging cable.

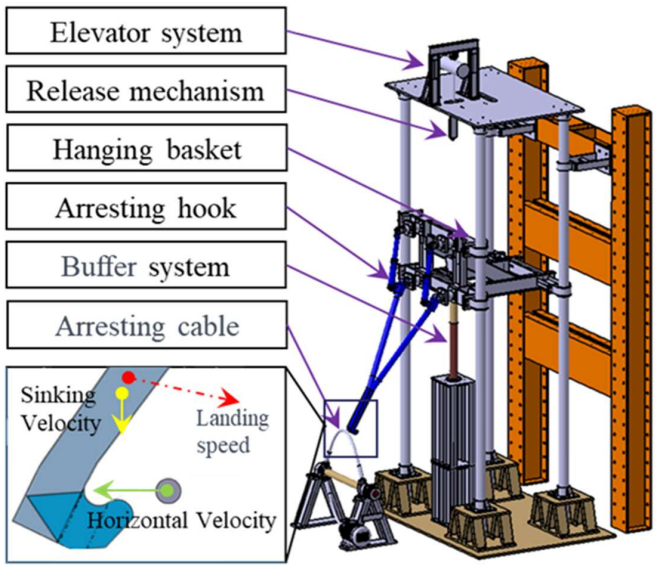

Figure 11. Arresting hook engaging arresting cable test.

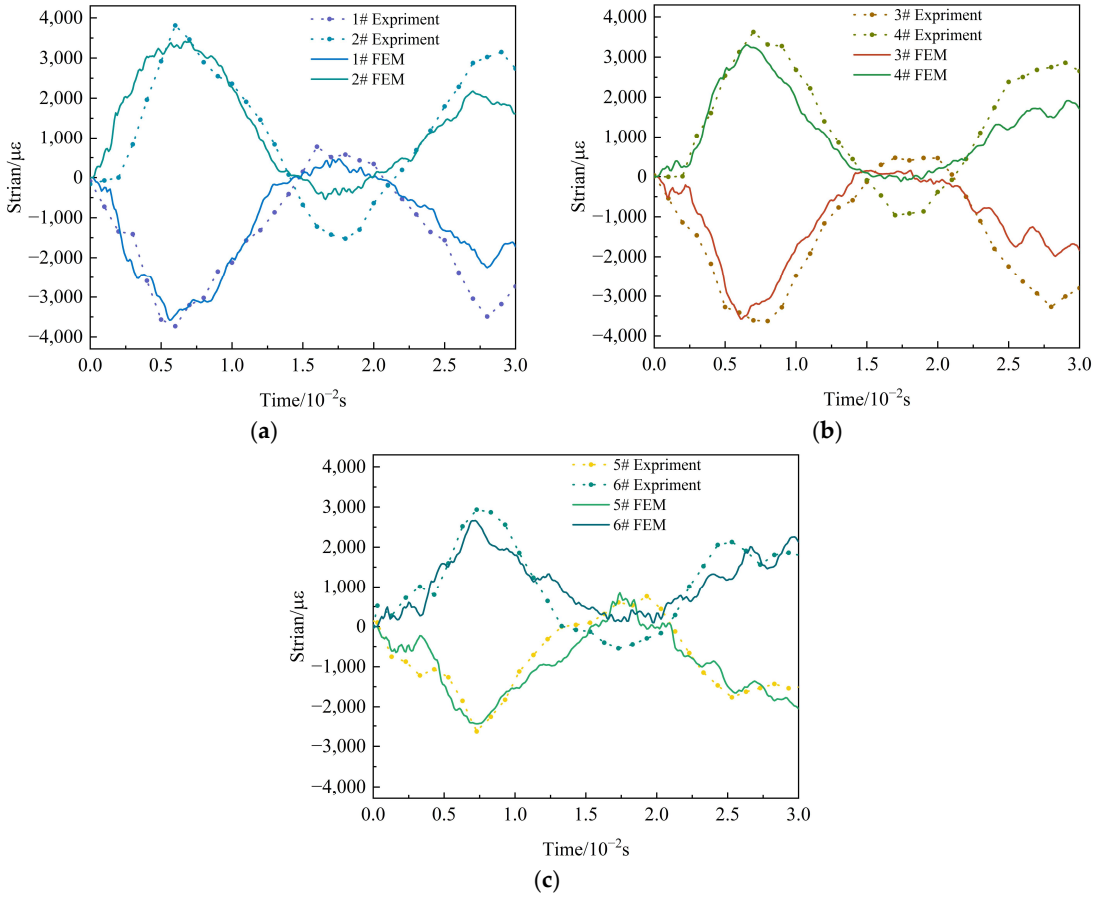

Figure 12. Comparison of simulated and experimental strain results at the moment of impact of the arresting hook at case 2: (**a**) Comparison between simulation and test of strain on the upper and lower surfaces of the lower end of the hook arm; (**b**) Comparison between simulation and test of strain on the upper and lower surfaces of the middle of the hook arm. (**c**) Comparison between simulation and test of strain on upper and lower surfaces of the upper end of hook arm.

Table 7. The maximum strain of the arresting hook engaging arresting cable at landing case 2.

Strain Gauge Location	Maximum Strain με		Error Value
	FEM	Experiment	
1#	−3415.99	−3772.05	9.44%
2#	3612.38	3851.38	6.21%
3#	−3615.21	−3665.95	1.38%
4#	3305.93	3664.48	9.78%
5#	−2447.35	−2663.64	8.12%
6#	2684.99	2966.02	9.48%

4. Dynamic Response Analysis of Arresting Hook Engaging Arresting Cable

4.1. Effect of Different Arresting Cable Models on the Dynamic Response of Arresting Hook Engaging Arresting Cable

This paper proposes a parameter inversion method for modeling the arresting cable and applies it to the transient dynamics model of the arresting hook and cable. Many scholars [17–20] have studied the stress state of the arresting cable during the arresting process, assuming the cable's flexibility and bending properties can be ignored. However, this assumption can result in significant deviations when analyzing the dynamic response of the arresting hook during cable impact. In this paper, we also modeled such cables, and the first type of steel element is consistent with this paper, and the second type of cable element is a beam element. The material parameters for the two types of cables are shown in Table 8. The three cable models were placed into the same transient dynamics model of the arresting hook and cable under the same conditions, and the three simulation results were compared, as shown in Figure 13. The transient dynamic results of the arresting hook arm when the arresting hook engages different arresting cables. In the figure, the solid steel cable with an elastic parameter of E = 210,000 MPa is called a rigid steel cable, the beam element cable is called the Beam cable, and the cable obtained through parameter inversion is called the flexible cable.

Table 8. Rigid Cable Material Parameters.

Cable Section Radius mm	Density ρ g/cm^3	Young's Modulus MPa	Poisson's Ratio	Element Type
19.5	5.45	210,000	0.3	C3D8R
19.5	5.45	210,000	0.3	B31

Figure 13 shows the strain curves at the hook arm monitoring point of the arresting hook and suspension cable at the same landing speed, and Table 9 compares the peak values of the three types of steel cables. From the figure and table, it can be seen that when the arresting hook impacts the flexible steel cable, the peak strains at various parts of the hook arm are all smaller than those when impacted by the other two types of steel cables, and the maximum error even exceeds 100%. Therefore, it is unreasonable to directly assume the arresting cable as a beam with metallic elastic parameters in the modeling process without considering the influence of the twisted structure and bending stiffness of the arresting cable.

When the arresting hook impacts the rigid steel cable and beam element steel cable, the error of the peak strain values at the middle and lower ends of the hook arm is within 2%, and the curve shapes are similar. The beam curve lags behind by 0.002 s, indicating that there is hysteresis in the contact process between the beam element and solid element. The stress state at the arresting hook root is different for all three impacts. The rigid steel cable causes a large strain at the root of the arresting hook, while the strain growth of the flexible steel cable and the beam element both lagged behind by 0.003 s, and the strain of the beam element remained above 1500 με for 0.01 s, while the strain of the flexible

steel cable quickly propagated backwards and had a distinct peak. This situation results in less damage to the connection between the arresting hook and the fuselage. During the simulation of the impacts of the three types of steel cables, the first peak of the curve ended at around 0.015 s, indicating that the elastic parameters of the steel cable only affect the intensity of energy transfer, not the time course of energy transfer. Therefore, the material does not affect the time course of the arresting hook being hooked onto the arresting cable.

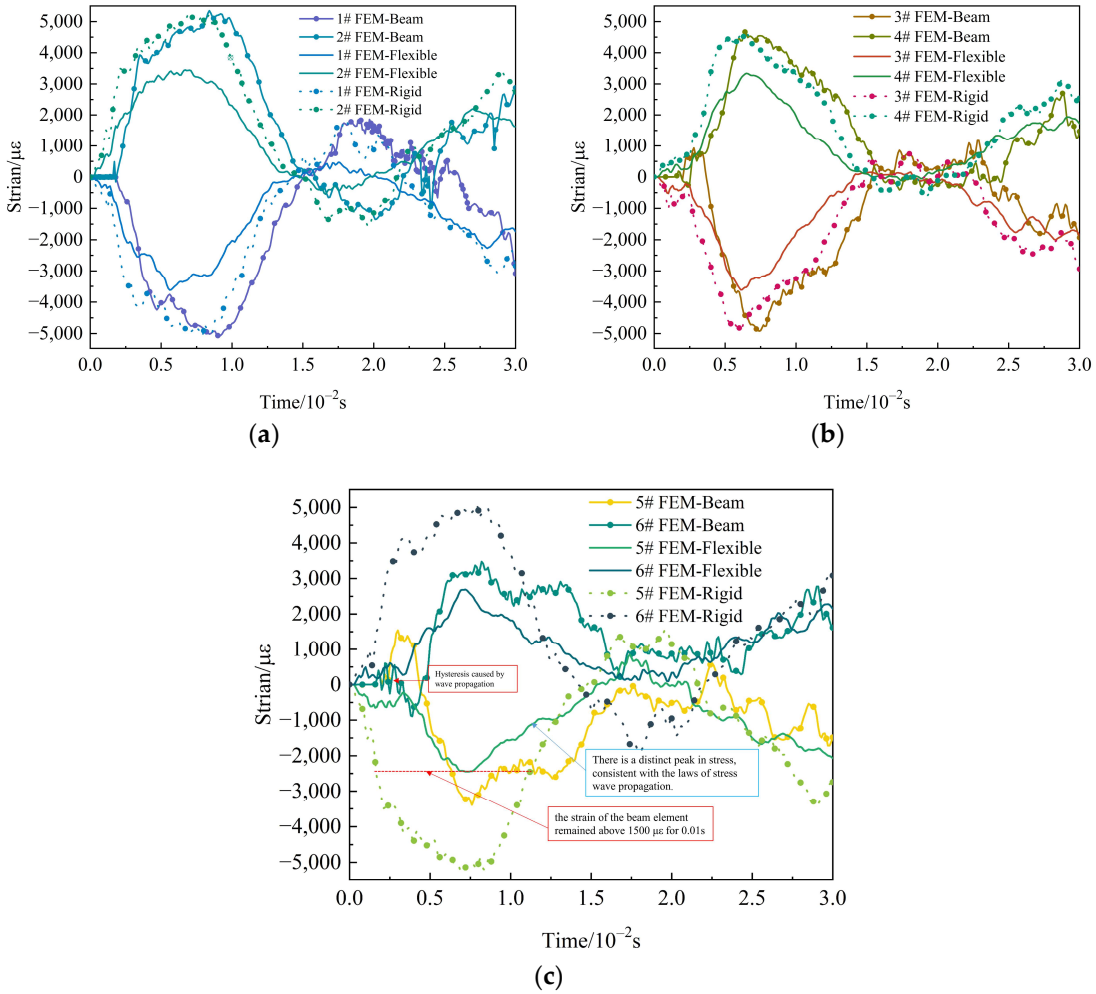

Figure 13. Transient dynamic analysis of the arresting hook arm in case 2 when engaging different cables: (**a**) Comparison of upper and lower surface strains at the lower end of the hook arm under rigid and flexible assumptions; (**b**) Comparison of upper and lower surface strains in the middle of the hook arm for rigid and flexible assumptions; (**c**) Comparison of the upper and lower surface strains in the middle of the hook arm under both rigid and flexible assumptions.

Table 9. Strain of the hook arm of the arresting hook when engaging the arresting cable of different materials in landing case 2.

Strain Gauge Location	Maximum Strain Mε			Error Value with Flexible Steel Cable	
	Beam	Rigid	Flexible	Beam	Rigid
1#	−5091.73	−5092.91	−3415.99	49.06%	49.09%
2#	5347.63	5311.34	3612.38	48.04%	47.03%
3#	−4904.35	−4887.93	−3615.21	35.66%	35.20%
4#	4666.25	4600.46	3305.93	41.15%	39.16%
5#	−3394.83	−5309.31	−2447.35	38.71%	116.94%
6#	3477.93	5092.68	2684.99	29.53%	89.67%

Through the comparison shown in Figure 14, it was found that at the moment when the hanging cable impact process ends at 0.015 s, there is little difference in the yaw displacement between the two solid steel cables, with the rigid cable only 17% more than the flexible cable. However, during the transient arrest process, the deformation of the flexible cable is transmitted to both sides from the center of the hanging cable in a more realistic manner, closer to the actual motion state of the arrest cable, while the rigid cable maintains a bow-shaped deformation with increasing distance from the hanging point on both sides. Since the reaction force of the arrest cable is small at the moment of the hook cable impact, the bending stiffness of the arrest cable affects the flexibility of the hanging cable during the hanging process, as can be seen from the simulation results.

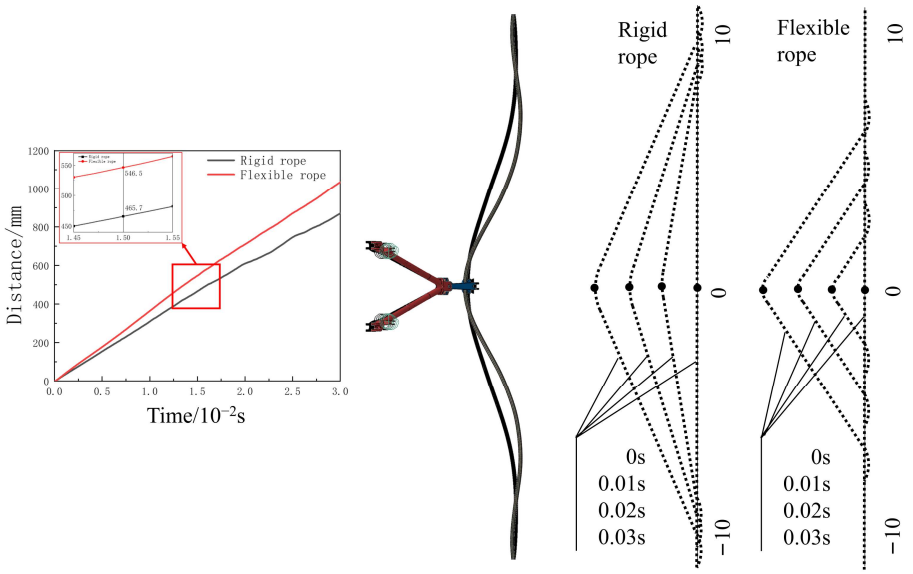

Figure 14. The state of the arresting process of different materials arresting cable.

4.2. Analysis of Dynamic Response of Arresting Hook in Aircraft Arresting and Hooking to Cable Arresting

In the previous analysis, the stress state of the hook arm at the moment of engagement with the arresting cable was discussed. However, many researchers often only study the load state of the arresting hook during the entire arresting process, from the hook successfully engaging the cable to the aircraft being brought to a stop. Assuming a symmetric engagement, the average load-displacement curve for the MK 7-3 arresting system during aircraft arrest, obtained from the US military standard MIL-STD-2066, was converted into a load-time curve using multi-body dynamics simulation. The load was then applied to the hook arm as shown in Figure 15, using a load-time curve instead of a static load. The strain state of the hook arm during the entire arresting process was calculated and is shown in Figure 16. The maximum strains at six monitoring positions were compared with the maximum stress at the moment of engagement, as shown in Table 10. It can be seen from the table that the stress peak during the engagement process is much higher than that during the aircraft arrest process, so it is unreasonable to ignore it in many studies. The accumulated bending deformation will also have a significant effect on the arresting hook. This indicates that part of the energy at the moment of engagement is absorbed by the bending deformation of the hook itself, part is absorbed by the arresting gear buffer, and part is absorbed by the arresting aircraft through the wave-like bending of the cable, consistent with the fluctuating nature of arresting loads mentioned in the US military standard MIL-STD-2066.

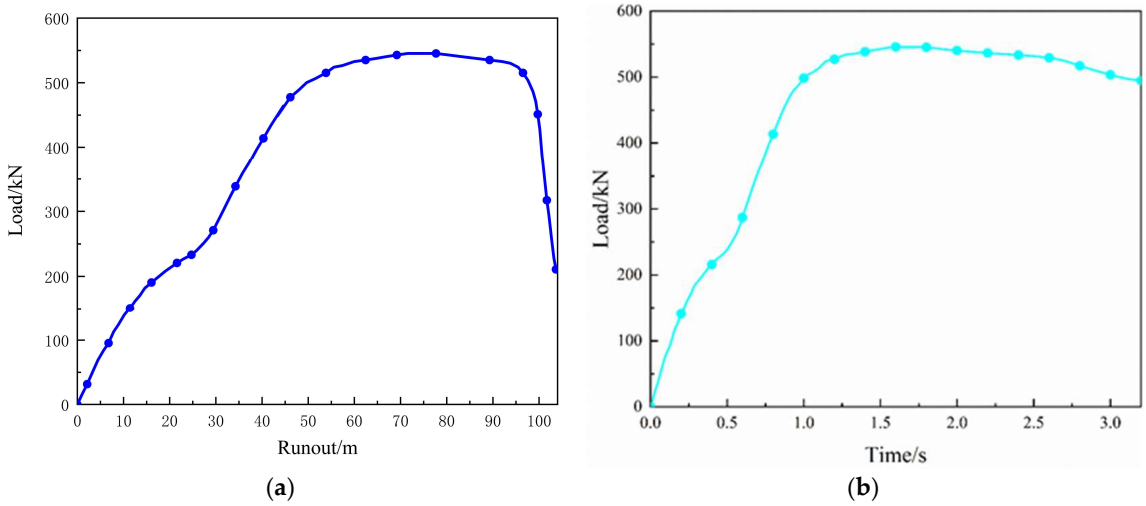

Figure 15. Load curve during aircraft arresting process on carrier deck: (**a**) Load-displacement curve of arresting machine; (**b**) Arresting load curve.

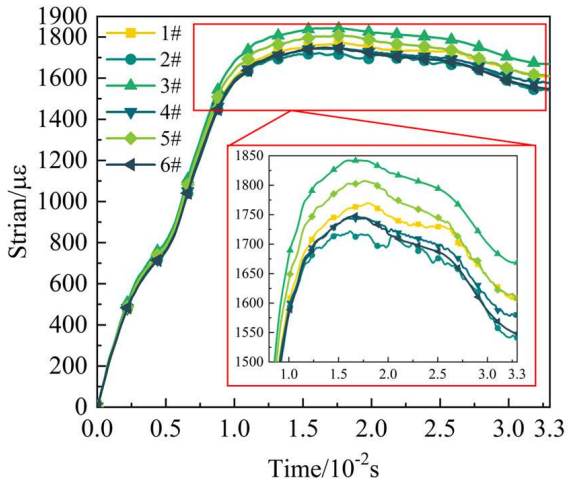

Figure 16. Arresting hook shank strain curve during aircraft arresting process.

Table 10. Comparison of maximum strain in the arresting hook under landing case 2 between aircraft arresting and hooking to cable arresting.

Strain Gauge Location	Maximum Strain με		Absolute Error (%)
	Arresting Cable	Arrested Landing	
1#	−3415.99	1769.60	293.04%
2#	3612.38	1721.79	109.80%
3#	−3615.21	1842.10	296.25%
4#	3305.93	1745.31	89.42%
5#	−2447.35	1807.37	235.41%
6#	2684.99	1748.24	53.58%

4.3. Effect of Flight Parameter Changes on the Dynamic Response of the Arresting Hook Engaging Arresting Cable

4.3.1. Dynamic Response of the Arresting Hook Engaging Arresting Cable at the Different Horizontal Velocity

As the carrier aircraft landing heading speed varies, the stresses on the arresting hook engaging the arresting cable impact change. From Figure 17, it can be seen that the stress magnitude at the same location of the arresting hook arm increases with the increase in

speed at different speeds, and the higher the speed the earlier the peak point appears. The peak stress between samples increases by about 130 ± 3 MPa for every 25% increase in velocity, and the line shape of the curve resembles that of the impact period. Figure 18 shows the stresses at several monitoring points for the sample heading speed of 51.44 m/s. The stresses at the lower and middle of the hook arm are larger than those at the upper end of the hook arm, and the stresses at the upper surface of the lower and middle of the hook arm are larger with a peak value of 771.39 MPa, while the stresses at the upper part of the hook arm near the joints of the arresting hook buffer become significantly smaller with a peak value of 523.26 MPa, indicating that the stresses at the impact of the lanyard at the moment of impact, the arresting hook arm produced bending elastic deformation, and the stress at the upper end of the arresting hook arm was smaller.

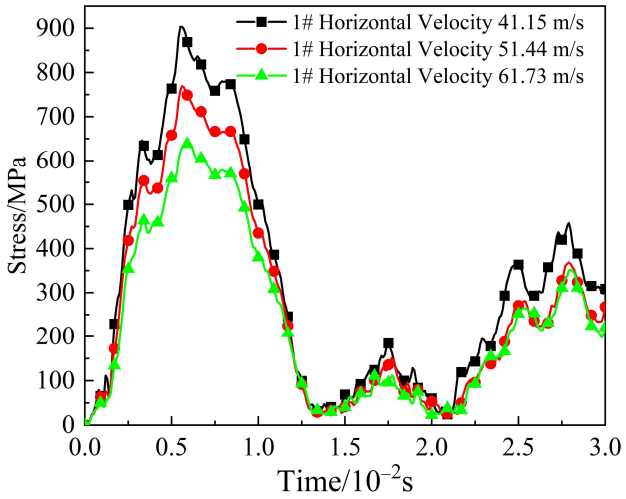

Figure 17. Stress at position 1# at different speeds.

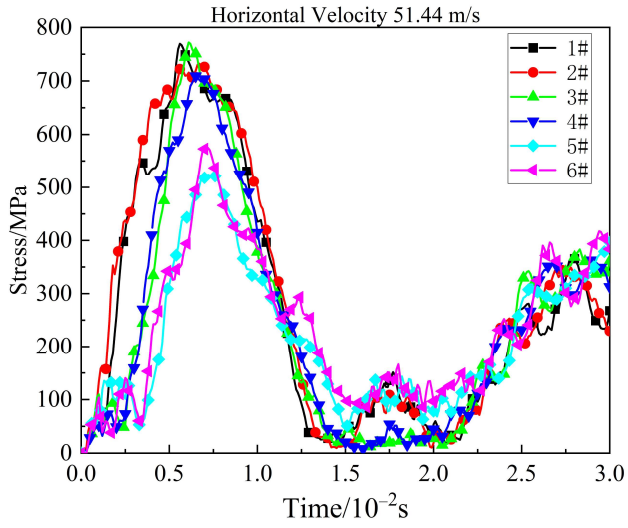

Figure 18. Stress at different positions at a horizontal speed of 51.44 m/s.

4.3.2. Dynamic Response of the Arresting Hook Engaging Arresting Cable at Different Yaw Angles

Figure 19 shows the comparison between the 16° yaw to the left state and the centered arresting state when the arresting hook engages arresting cable, with positive left yaw and negative right yaw in the graph. After 0.03 s after hanging the cable, the hook and cable heading displacement do not change much, however, the lateral displacement has started to show a deviation of 0.315 m, and the movement of the cable has changed. Since the hook arm is symmetrically laid out, the stresses at the lower 1# position of the hook arm are

studied when the yaw angle is ±16° and when the alignment is arrested. Table 11 shows that the time of the contact process between the yaw arresting and the center arresting hook and cable is the same for the same heading speed and sinking speed. When yawing, the stress on the hook arm is large on the side of the yaw angle. When the yaw angle is ±16°, the stress of the maximum size of the hook arm is 15.4% higher than that on the middle arresting, which is less than the yield strength of the arresting hook. It shows that the arresting system works well when the heading speed of the shipborne aircraft is 51.44 m/s.

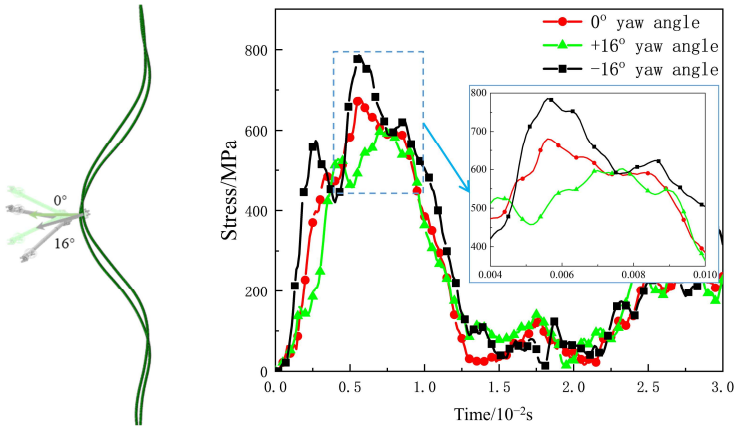

Figure 19. Stress curve of the arresting hook arm of the arresting hook engaging arresting cable in yaw condition.

Table 11. Stress state of the arresting hook arm of the arresting hook engaging arresting cable in different yaw conditions under landing case 2.

Yaw Angle °	1# Maximum Stress MPa	Lateral Displacement of Hook and Cable Engagement Position/mm
4	775.7	80.7
8	718.8	157.7
12	701.7	239.2
16	678.5	314.7
0	769.4	0
−4	782.3	−81.4
−8	876.5	−158.2
−12	887.9	−239.4
−16	895.8	−315.0

4.3.3. Dynamic Response of the Arresting Hook Engaging Arresting Cable at Different Initial Positions

In addition, this paper studies the mechanical properties of the arresting hook under different contact states. Firstly, we analyze the mechanical properties when the arresting hook engages the arresting cable at varying deck angles; secondly, we analyze the mechanical properties when the arresting hook engages the arresting cable at different initial positions.

Usually, the arresting hook deck angle is lower than 65 degrees when the carrier aircraft is landing. To study the effect of the angle change on the mechanical properties of the arresting hook engaging the arresting cable, this paper begins with a deck angle of 62° and reduces it in units of 2° until it reaches 52°. Based on the analysis of the six monitoring points on the hook arm of the arresting hook, it is concluded that there is no obvious difference in the curve of the instantaneous stress of the arresting hook rope at different angles with time, so this article only shows the peak of the curve, as shown in Table 12. The table shows that when the arresting hook and the arresting cable are normally engaged, the change in deck angle has little effect on the mechanical properties of the arresting hook.

Table 12. A comparison of the peak stress values of the hook arm of the arresting hook engaging the arresting cable at different deck angles.

Case	Angle/°	1#Stress/MPa	2#Stress/MPa	3#Stress/MPa	4#Stress/MPa	5#Stress/MPa	6#Stress/MPa
A0	62	781.64	758.83	742.84	730.07	561.00	563.94
A2	60	781.64	747.83	750.47	716.61	517.40	571.15
A4	58	747.36	743.47	749.00	721.27	542.70	578.99
A6	56	745.29	727.63	737.37	730.88	523.88	561.14
A8	54	769.03	737.82	712.70	708.99	527.92	580.45
A10	52	747.45	699.74	696.83	709.95	521.41	549.56

Stress transfer in the arresting hook is affected by the initial contact position between the arresting cable and the hook head. A total of six initial contact situations are considered in this paper. In each condition, the initial cable position is 10 mm higher vertically, and the horizontal direction is unchanged, as shown in Figure 20. Figure 21 shows the stress-time curves for the 1# position of the hook arm under different conditions. Among them, the three conditions of a, b, and c are successful of the arresting hook engaging the arresting cable. The arresting cable is impacted by the hook head in condition c, thereby gaining an initial velocity in the same direction, and when it is impacted by the hook throat again, the impact energy is smaller than in conditions a and b. In the scenarios of d, e, and f, the arresting hook fails to engage with the arresting cable. Among these, the hook arm in condition d experiences higher internal stress compared to the other five conditions. The hook arm in condition d has a higher stress than those in the other five conditions, and the peak stress data at each position are shown in Table 13. From the chart, we can see that condition a and b have basically the same stress; condition d has the most stress; the peak stress of six monitoring points is 10–20% higher than that of conditions a and b; and condition c, e, and f are relatively gentle, which does not have much effect on the arresting hook.

Table 13. A comparison of the peak stress values of the hook arm of the arresting hook engaging the arresting cable at different positions of initial contact.

Contact Condition	1#Stress/MPa	2#Stress/MPa	3#Stress/MPa	4#Stress/MPa	5#Stress/MPa	6#Stress/MPa
a	754.94	728.49	742.19	686.70	511.97	527.03
b	760.57	737.16	673.72	635.81	481.40	523.63
c	656.20	705.48	536.52	517.90	389.00	400.33
d	838.48	838.48	836.18	777.48	599.32	625.58
e	688.45	675.80	724.86	666.95	537.08	555.10
f	524.98	542.99	621.23	559.59	445.57	438.22

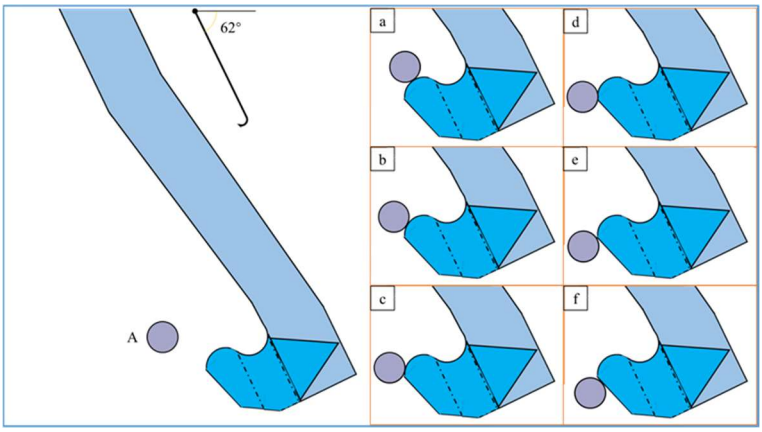

Figure 20. Angle of deck and initial position before arresting hook engages arresting cable.

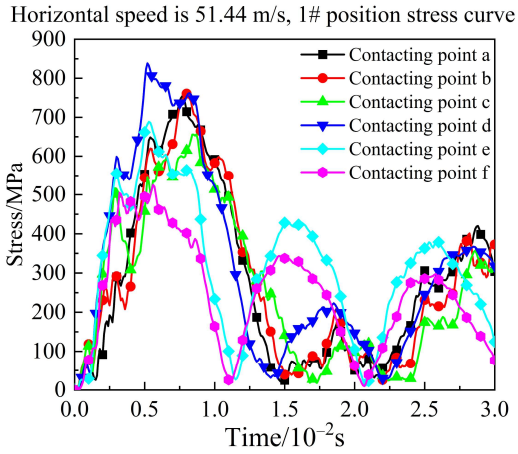

Figure 21. At different initial contact points, comparison of stress curves of 1# during the meshing process of arresting hooks and arresting cables.

Considering the large stress in condition d as shown in Figure 22, the arresting hook head is chamfered in this paper, and the radius of the chamfering is 10 mm. As shown in Figure 23, stress data of point 1# before and after chamfering, the stress peak value after chamfering is 761.94 MPa, which is reduced by 9%. According to the study, the parts of the arresting hook head that come into contact with the arresting cable should be rounded to improve mechanical transmission.

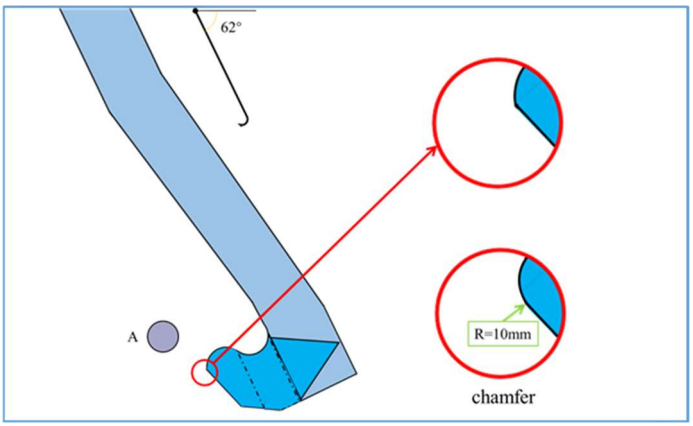

Figure 22. The hook head of the arresting hook is chamfered.

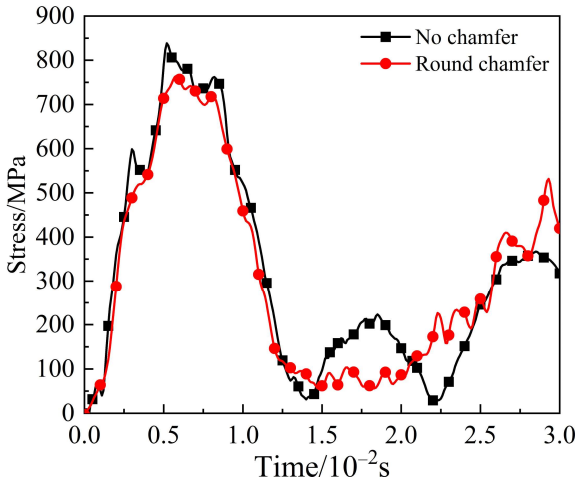

Figure 23. Point 1# stress curve during initial contact between arresting hook and arresting cable with and without chamfer.

5. Conclusions

Addressing the challenges of modeling the transient dynamics of arresting hooks and cables, this study introduces the parameter inversion method to model the arresting cable and applies it to the transient dynamics model of the arresting hook and cable. The feasibility of the arresting cable model and its application to the transient dynamics model of the arresting hook and cable are validated through arresting hook and cable impact tests. Based on this, some important conclusions about the dynamics of arresting hooks and cables are obtained:

(1) The method of establishing the arresting cable model using the parameter inversion method is feasible and can be used in the transient dynamics model of arresting hooks and cables, providing a method and idea for the transient dynamics model of arresting hooks and cables.
(2) Simple modeling of the arresting cable as an isotropic metal rod with an elastic modulus of E = 210,000 MPa will result in significant errors in the transient dynamics process of arresting hooks and cables, with maximum errors exceeding double the actual value.
(3) In the arresting hook and cable process, a 2° increase in the yaw angle of the aircraft will increase the stress on the arresting hook arm by 2%; a 2° increase in the deck angle of the arresting hook will increase the stress on the arresting hook arm by 1%; a 25% increase in the aircraft's cruising speed will increase the stress on the arresting hook arm by 20%. In addition, the initial position of the arresting hook and cable before engagement will affect the stress curve of the arresting process, with the case where the arresting cable collides with the arresting hook head resulting in an 11% increase compared to normal engagement.

The research results of this paper are of great significance for improving the design optimization of the structural strength of the functional components of the naval aircraft arresting system, and they provide theoretical guidance and technical reserves for subsequent related studies.

Author Contributions: Conceptualization, L.L.; methodology, L.L., Y.P. and X.W.; software, L.L., Y.W. and Y.P.; validation, L.L., Y.W. and Y.P.; formal analysis, L.L., X.W. and H.N.; investigation, L.L., Y.W. and Y.P.; resources, L.L., Y.P., X.W. and H.N.; data curation, L.L. and Y.W.; writing—original draft preparation, L.L.; writing—review and editing, L.L., Y.P., Y.W., X.W. and H.N.; visualization, L.L.; supervision, H.N.; project administration, H.N.; funding acquisition, X.W. All authors have read and agreed to the published version of the manuscript.

Funding: This study was co-supported by Natural Science Foundation of Jiangsu Province: BK20220910; National Natural Science Foundation of China: 52202441; National Defense Outstanding Youth Science Foundation: 2018-JCJQ-ZQ-053.

Conflicts of Interest: The authors declare no conflicts of interest.

References

1. Zhang, S.Q.; Wang, H.M. Summary Report on Automatic Carrier Landing System. *Aircr. Des.* **2022**, *42*, 20–24.
2. Naval Air Engineering Center. *Mil-Std-2066 (AS) Military Standard Catapulting and Arresting Gear Forcing Functions for Aircraft Structural Design*; Naval Air Engineering Center: Lakehurst, NJ, USA, 1981.
3. Yang, Q.W. Research on flight measurement method of a carrier-based aircraft arresting hook loads. *Acta Aeronaut. Astronaut. Sin.* **2015**, *36*, 1162–1168.
4. Zhang, Y.L. Design and Analysis of Static Strength Test of Arresting Hook. *Eng. Test* **2022**, *01*, 62–64.
5. Ringleb, F.O. *Cable Dynamics*; Naval Air Engineering Facility Engineering Department: Lakehurst, NJ, USA, 1956.
6. Gibson, P.T.; Cress, H.A. *Analytical Study of AIRCRAFT Arresting Gear Cable Design*; Battelle Memorial Institute: Columbus, OH, USA, 1965.
7. Gibson, P.T.; Alexander, G.H.; Cress, H.A. *Validation of Design Theory for Aircraft Arresting-Gear Cable*; Battelle Memorial Institute Columbus OH Columbus Laboratories: Columbus, OH, USA, 1968.

8. Dodson, M.; Gibson, P.T.; Clark, G.A.; Cress, H.A.; Battelle Memorial Inst Long Beach Ca Long Beach Ocean-Engineering Facility. *Investigation of the Influence of Hook Abrasion and Wire Materials on the Useful Service Life of Deck Pendants*; Battelle Memorial Institute Laboratories Long Beach CA Ocean-Engineering Facility: Columbus, OH, USA, 1970.
9. Gao, Z.J. A discussion of bounce kinematics of aircraft arresting hook and cable dynamics. *Acta Aeronaut. Et Astronaut. Sin.* **1990**, *11*, B543–B548.
10. Liang, L.; Wan, C.; Xun, P. Study on the dynamic performance of aircraft arresting cable. *Acta Aeronaut. Et Astronaut. Sin.* **2013**, *34*, 833–839.
11. Liang, L.; Chen, W.; Panpan, X. Dynamic analysis of aircraft arresting gear based on finite element method. In Proceedings of the 2011 International Conference on System Science, Engineering Design and Manufacturing Informatization, Guiyang, China, 22–23 October 2011; Volume 2, pp. 118–121.
12. Shen, W.H.; Zhao, Z.H.; Ren, G.X. Multi-body dynamic simulation of impact on cross deck pendant. *J. Vib. Shock* **2015**, *34*, 73–77.
13. Shen, W.; Ding, X.; Guo, S. Stress Simulation of the Purchase Cable. *Sci. Technol. Eng.* **2015**, *14*, 224–229.
14. Zhang, Q. *Research on Impact Dynamics and Test Method of Arresting Hook*; Nanjing University of Aeronautics and Astronautics: Nanjing, China, 2018.
15. Dang, X.Y.; Huang, C.G.; Feng, Z.Z. Dynamics Simulation Analysis of Carrier Aircraft Landing Arresting Based on PAM-CRASH. *Equip. Environ. Eng.* **2020**, *09*, 15–20.
16. Huang, K.; Yang, W.; Ye, X. Adjustment of machining-induced residual stress based on parameter inversion. *Int. J. Mech. Sci.* **2018**, *135*, 43–52. [CrossRef]
17. Yao, W.B.; Cheng, H. Determination of wire rope tension by means of three points loading flexure. *J. Exp. Mech.* **1998**, *13*, 79–84.
18. Abaqus, V. *6.14 Documentation*; Dassault Systemes Simulia Corporation: Johnston, RI, USA, 2014; Volume 651.
19. Qun, X. *Research on Bending Behavior of Parallel Steel Wire Cable*; Tianjin University School of Civil Engineering: Tianjin, China, 2019.
20. Hong, K.J. *Dynamic Interaction in Cable-Connected Equipment*; University of California: Berkeley, CA, USA, 2003.
21. Sun, Q.; Liu, R.; Liang, K. Impact Fatigue Life Prediction for Notched Specimen of Steel AerMet100 Subjected to High Strain Rate Loading. *Int. J. Appl. Mech.* **2018**, *10*, 1850030. [CrossRef]